Planetary Physics

Lunar Seismology: Determining the Internal Structure of the Moon

Christopher Winta*
Freie Universität Berlin, Fachbereich Physik
Supervisor: Dr. Kai Wünnemann†
Museum für Naturkunde, Leibniz-Institut für Evolutions- und Biodiversitätsforschung

December 30, 2013

Table of Contents

*christopher.winta@fu-berlin.de
†kai.wuennemann@mfn-berlin.de

1 Introduction

Since its development in the early 1900's, seismology has been an effective tool to determine the internal structure of the earth. For example, in 1906, Richard Oldham managed to detect the presence of the earth's liquid outer core using seismological data by observing the so-called *seismic shadow zone* at source-receiver angular distances of about 104° to 140° in which no seismic waves can be detected after an earthquake. This is because seismic shear waves (or secondary waves) cannot penetrate the liquid outer core while compressional waves (or primary waves) are refracted [1]. Later, in 1909, with more seismological data at hand, Andrija Mohorovičić was able to observe the *Mohorovičić discontinuity* (or M-discontinuity or MOHO) which is a rapid wave velocity transition at an average depth of less than 54 km and marks the borderline between the earth's crust and mantle [2].

In the following decades, the increasing number of seismological observations and records finally lead to Adam M. Dziewonski's and Don L. Anderson's *Preliminary Reference Earth Model* (PREM) from 1981 which describes how the earth's velocity and density structure depends on depth [3]. Figure 1 shows a plot of the PREM data. Besides travel times of obser-

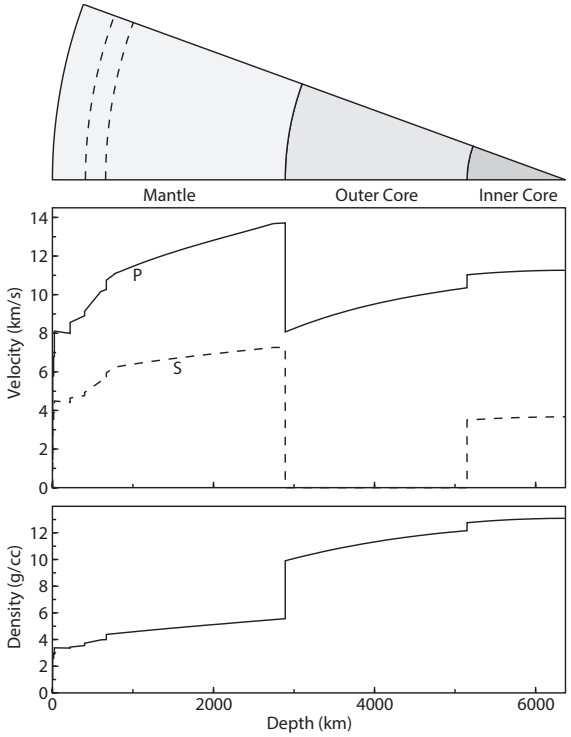

FIG. 1: Plotted version of PREM (1981). Even recent models are in very good accordance with PREM, except for small discrepancies in the upper mantle region. Data from [3], taken from [4]

ved seismic waves, the model also fits a variety of different boundary conditions like, for example, the earth's total mass and its moment of inertia which can be obtained through astronomical observations, making this model even more relevant.

Beginning in 1969 with the first manned landing on the moon during the Apollo 11 mission, NASA started to deploy seismometers on the moon's surface allowing the same measurements that have been conducted on earth before. During the following missions of Apollo 12, 14, 15 and 16, NASA built up a seismic network of four stations that returned seismic data on approximately 10,000 deep moonquakes, 28 shallow moonquakes, 1,800 meteoroid impacts and 9 artificial impacts over the nearly eight years of operation and is known as the *Apollo Seismic Passive Experiment* (PSE) [5, 6].

This text shall deliver a short but keen insight into the scientific methods of modern seismology. Thereto, chapter 2 will give an overview of the physics and mathematics involved to gain information about the inner structure of a planetary body from seismological observations. Chapter 3 will then provide some technical details on the Apollo missions and on how seismic data can be acquired on the moon. Chapter 4 will present two possible analysis methods using the example of N. R. Goins', A. M. Dainty's and M. N. Toksöz's work *"Lunar Seismology: The Internal Structure of the Moon"* [7]. Ultimately, Chapter 5 will give a short outlook to the future of lunar seismology.

2 Theoretical Basics

The following chapter shall give a rough idea – without providing mathematical and technical details – on how to gain information about the internal structure of a planetary body. Since its purpose is to illustrate the nature of seismology's mathematical framework, it is restricted to a one dimensional velocity gradient in a planar body which often models real world problems satisfactorily well. A generalization to three dimensions and roundly shaped bodies is a purely mathematical (and tedious) exercise and yields no further perception of the physical nature. Also, other perturbations like *low velocity zones* (LVZ) and scattering effects are not covered in this short outline which is mainly taken from Peter M. Shearer's *"Introduction to Seismology"* [4].

2.1 Seismic Wave Types

Seismic waves are, generally speaking, a form of energy that travels through an planetary body. They are usually caused by earthquakes, impacts, explosions or volcanic eruptions. There are basically two seismic wave types, namely P waves and S waves.

P (or longitudinal) waves are compressional pressure waves, whereas S (or transverse) waves are pure shear waves. Their propagating natures are depicted in figure 2.

The nomenclature P and S stands for *"Primary"* and *"Secondary"* and stems from the fact that P waves travel faster through solids than S waves and are therefor registered first after an earthquake.

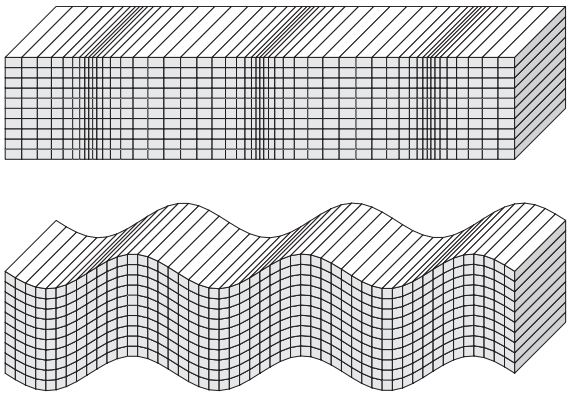

FIG. 2: Harmonic P wave (top) and S wave (bottom) propagating horizontally across the page. Note that P (longitudinal) propagation – unlike S (transverse) propagation – causes a volume change in the material. Compared to real planetary objects, the deflections shown are highly exaggerated. Taken from [4].

2.2 Velocity

In order to do seismologic calculations, we must develop a mathematical model of the propagation velocity of plane waves in a solid. This mathematical model is already given by the field of *linear elasticity* which provides mathematical descriptions on how a solid deforms and becomes internally stressed.

In linear elasticity, homogeneous and isotropic materials are characterized by their so-called *Lamé parameters* λ and μ which denote, respectively, the first Lamé parameter and the shear modulus (or modulus of rigidity). These two parameters are related via the bulk modulus (or modulus of incompressibility) κ:

$$\kappa = \lambda + \frac{2}{3}\,\mu. \tag{2.1}$$

These parameters allow a mathematical description of the plane wave velocities v_P and v_S for both, P and S waves respectively, which are given by

$$v_P = \sqrt{\frac{\lambda + 2\mu}{\rho}} = \sqrt{\frac{\kappa + \frac{3}{4}\mu}{\rho}} \quad \text{and} \tag{2.2}$$

$$v_S = \sqrt{\frac{\mu}{\rho}}, \tag{2.3}$$

where ρ denotes the material's mass density [4].

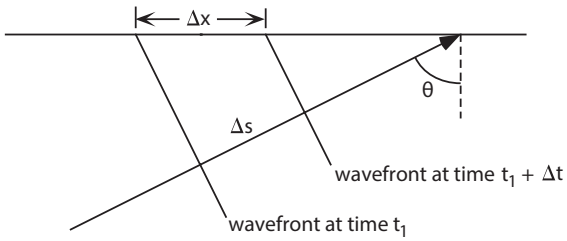

FIG. 3: A seismic plane wave traveling with constant velocity v under an angle θ relative to the surface's perpendicular. Taken from [4].

A derivation of these formulas will not be shown in this text, but can be found in [8].

2.3 Ray Theory and Travel Times

Seismic *ray theory* provides a relatively simple, yet powerful, model we can use to calculate travel times of seismic waves using the velocity relations we obtained in the previous section. Additionally, it comes in handy that seismic ray theory is mostly analogous to its optical counterpart which allows a more intuitive understanding.

A big advantage of ray theory (and in particular of the ray tracing routines described below) is that it is easy to implement for computer-assisted calculations. However, it is a very simple model and naturally has its limitations when it comes to describing so-called "non-geometrical" effects such as head waves or refracted waves.

2.3.1 Snell's Law

Assuming a seismic plane wave propagating with constant velocity v under an angle θ relative to the surface's perpendicular, we have

$$\Delta s = \Delta x \cdot \sin\theta, \tag{2.4}$$

where Δs is the distance separating the same wavefront at given times t_1 and $t_1 + \Delta t$ and Δx the corresponding distance on the surface (see figure 3).

Using $\Delta s = v\Delta t$ and defining the so-called *slowness* $u = v^{-1}$, we get

$$\frac{\Delta t}{\Delta x} = \frac{\sin\theta}{v} = u \cdot \sin\theta \equiv p, \tag{2.5}$$

where p denotes the *ray parameter* which is also called *horizontal slowness* since it represents the

projection of u on the surface plane. Note that p can be measured directly by timing the arrivals of the wavefront at two points separated by Δx.

The next step is to consider a plane wave striking a interface between two layers of homogeneous, but different plane wave velocities v_1 and v_2. As figure 4a shows, the direction of propagation must change at the interface in order to conserve the continuity of the wavefronts at the borderline between layers.

Since the ray parameter p with respect to the interface is the same for both velocities v_1 and v_2, we can use equation 2.5 to formulate

$$p = u_1 \cdot \sin\theta_1 = u_2 \cdot \sin\theta_2, \tag{2.6}$$

where θ_1 and θ_2 denote the respective ray angles from the vertical (see figure 4a). Notice that this is in perfect analogy with *Snell's law of refraction* of geometrical optics.

2.3.2 Continuous Velocity Gradients

We can now generalize our findings about seismic wave refraction by considering a series of layers of increasing wave velocities as shown in figure 4b. Applying equation 2.6 yields

$$p = u_1 \cdot \sin\theta_1 = u_2 \cdot \sin\theta_2 = u_3 \cdot \sin\theta_3 = \cdots . \tag{2.7}$$

As the velocity increases with each layer, θ also increases, forcing the ray into a bent trajectory until it reaches its so-called *turning point* with $\theta = 90°$.

Now, it is easy to imagine a continuous velocity gradient instead of a layered material by assuming an infinitesimally small distance $\mathrm{d}z$ between interfaces. Using that p is constant throughout the whole ray path (see equation 2.7), we know for any given u and θ that

$$p = u_0 \cdot \sin\theta_0 = u \cdot \sin\theta, \tag{2.8}$$

where u_0 is the *initial slowness* and θ_0 the *takeoff angle* of the ray. Note that $p = u_{\mathrm{tp}}$, where u_{tp} is the slowness at the turning point as $\sin(90°) = 1$.

Most generally, plane wave velocity increases with depth z in most solid planetary bodies. Figure 6 shows ray paths for different ray parameters p and a linearly increasing plane wave velocity $v(z)$. The velocity gradient causes the ray to turn back towards the surface while smaller ray parameters result in deeper penetration depths and therefor in longer travel distances X along the surface.[1]

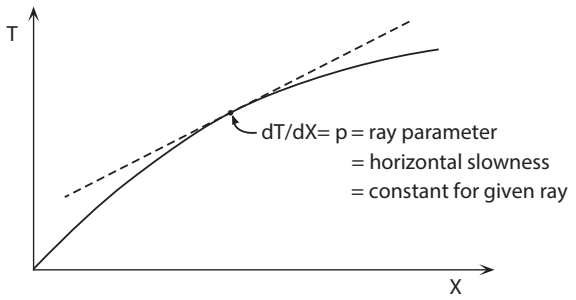

FIG. 5: Travel time curve for a model in which velocity increases with depth. One point on the curve corresponds to one given ray path whose ray parameter p equals the slope in that point of the curve. Taken from [4].

The travel time properties of a given material can be characterized by its *travel time curve* which illustrates the dependence of the total travel time T on the total travel distance X along the surface. If the velocity increases with depth, the time travel curve will qualitatively look like figure 5.

2.3.3 Travel Distance and Time

We can define the slowness vector $\mathbf{s}$ which has the length u and is directed along the propagation direction of a given ray. This slowness vector $\mathbf{s}$ can be split up in its horizontal and vertical components $\mathbf{s}_x$ and $\mathbf{s}_z$. The length of $\mathbf{s}_x$ is obviously given by the horizontal slowness

$$p = |\mathbf{s}_x| = u \cdot \sin\theta, \tag{2.9}$$

whereas the vertical slowness $|\mathbf{s}_z|$ can be analogously defined as

$$\eta = |\mathbf{s}_z| = u \cdot \cos\theta \tag{2.10}$$

(see figure 7a). In the same manner, we can as-

[1] The described 1-dimensional model does not provide any explanation on why the ray would bend back towards the surface after the turning point, since it travels parallel to the velocity gradient. Still, this is an experimentally observed effect caused by reflection near the turning point.

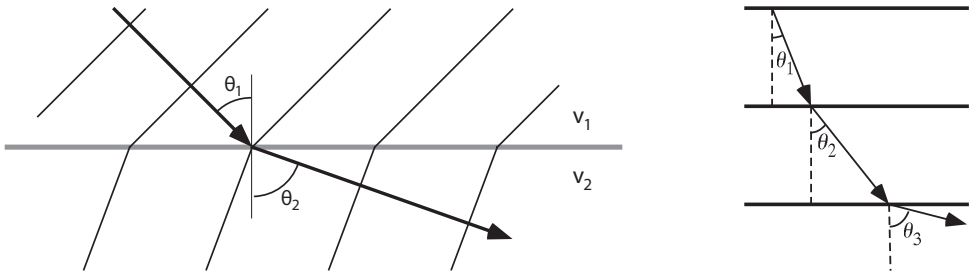

(a) (b)

FIG. 4: (a) A seismic planewave must change its direction of propagation at a interface between two layers of different velocities $v_1 < v_2$. The time difference Δt between plotted wavefronts is constant. (b) A series of layers of increasing velocities therefor causes stepwise diffraction of the seismic plane wave. Taken from [4].

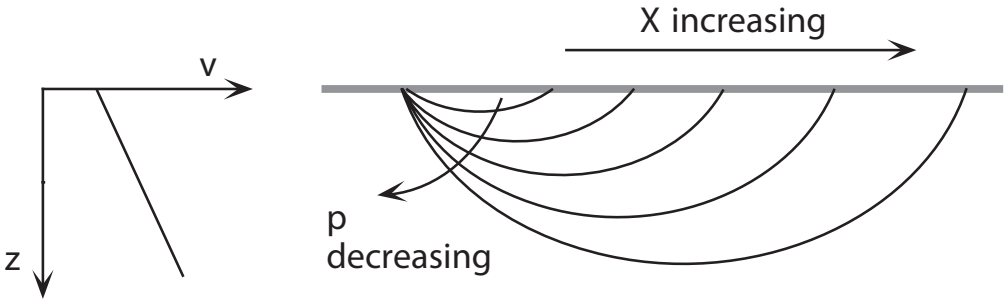

FIG. 6: Ray paths for different ray parameters p. A linearly increasing plane wave velocity $v(z)$ results in semicircular ray paths. Smaller ray parameters p yield longer distances X. Every ray path corresponds to one point in a travel time curve. Taken from [4].

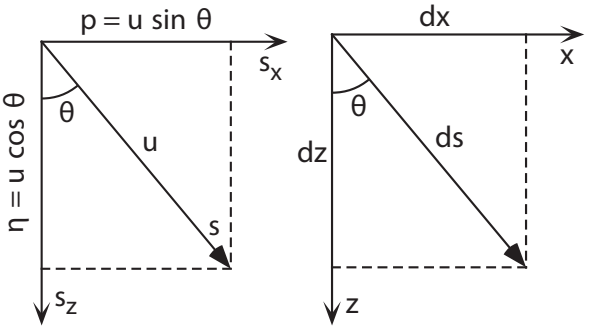

(a) (b)

FIG. 7: (a): Angle relations of the slowness vector **s**. (b): A length segment along the ray path ds and their horizontal and vertical components. Taken from [4].

sume an infinitesimally small length segment ds and its horizontal and vertical components dx and dz (see figure 7b).

With simple trigonometry we can now formulate the following relations:

$$\frac{\mathrm{d}x}{\mathrm{d}s} = \sin\theta \tag{2.11}$$

$$\frac{\mathrm{d}z}{\mathrm{d}s} = \cos\theta = \sqrt{(1-\sin^2\theta)}. \tag{2.12}$$

Using $p = u \cdot \sin\theta$, we get

$$\frac{\mathrm{d}x}{\mathrm{d}s} = \frac{p}{u} \tag{2.13}$$

$$\frac{\mathrm{d}z}{\mathrm{d}s} = \frac{\sqrt{u^2-p^2}}{u}. \tag{2.14}$$

We can use these expressions to calculate dx/dz:

$$\frac{\mathrm{d}x}{\mathrm{d}z} = \frac{p}{\sqrt{u^2-p^2}} \tag{2.15}$$

Integrating eventually gives us an expression for the horizontal distance X

$$X(p) = 2p\int_0^{z_{\mathrm{tp}}} \frac{\mathrm{d}z}{\sqrt{u^2(z')-p^2}}, \tag{2.16}$$

where z_{tp} is the depth of the turning point. We therefor integrate halfway along the ray path and use the symmetry around the turning point by doubling the result in order to get the total horizontal distance $X(p)$.

Similarly, using dt/d$s = u$ we can derive the expression

$$\frac{\mathrm{d}t}{\mathrm{d}z} = \frac{u^2}{\sqrt{u^2(z)-p^2}}. \tag{2.17}$$

Integrating and using the symmetry of the ray path once again finally yields

$$T(p) = 2\int_0^{z_{\mathrm{tp}}} \frac{u^2(z)}{\sqrt{u^2(z)-p^2}}\,\mathrm{d}z. \tag{2.18}$$

Equations 2.16 and 2.18 allow us to derive the total distance and the travel time, respectively, for a given ray with p in a slowness gradient $u(z)$.

2.4 Inversion of Travel Time Data

In a real world problem, we are more likely to know X and T from measurements and want to compute the corresponding slowness gradient $u(z)$.

The solution to a similar problem was found in 1826 by Niels Henrik Abel which is called *Abel integral* [9].[2] It states that the solution to an integral equation of the form

$$t(x) = \int_x^a \frac{f(\xi)}{\sqrt{\xi - x}}\,\mathrm{d}\xi \tag{2.19}$$

is given by

$$f(\xi) = -\frac{1}{\pi}\frac{\mathrm{d}}{\mathrm{d}\xi}\int_\xi^a \frac{t(x)}{\sqrt{x-\xi}}\,\mathrm{d}x. \tag{2.20}$$

If we use equation 2.16 and change the integration variable to u^2, we get

$$\frac{X(p)}{2p} = \int_{u_0^2}^{p^2} \frac{\mathrm{d}z/\mathrm{d}(u^2)}{\sqrt{u^2-p^2}}\,\mathrm{d}(\mathrm{u}^2), \tag{2.21}$$

where $u_0 = u(z=0)$. We can solve this integral equation by identifying $t(x) = X(p)/2p$, $x = p^2$, $\xi = u^2$ and $f(\xi) - \mathrm{d}z/\mathrm{d}(u^2)$ which makes this equation analogous to 2.19. Using Abel's solution yields

$$z(u) = -\frac{1}{\pi}\int_{u_0}^{u} \frac{X(p)}{\sqrt{p^2-u^2}}\,\mathrm{d}p. \tag{2.22}$$

Equation 2.22 can be rewritten using partial integration to give

$$z(u) = \frac{1}{\pi}\int_0^{X(u)} \cosh^{-1}(p/u)\,\mathrm{d}x. \tag{2.23}$$

This approach was derived in the 1900s independently by Gustav Herglotz, Emil Wiechert and Harry Bateman and is often referred to as the *Herglotz-Wiechert method* [10, 11, 12, 13].

[2] The original problem was to find the shape of a hill, given the time it takes a ball to roll up and back down the hill, as a function of the initial velocity of the ball.

3 Data Acquisition

All seismic data from the moon originate from the four stations set up during NASA's Apollo Missions 12, 14, 15 and 16 between 1969 and 1972 (see figure 8). Each Station consists of four seismometers: three long-period instruments (LP) with response peaks ranging from periods from 1 s to 10 s and one short-period instrument (SP) with a response peak at 8 Hz [14]. Some seismometers also include polarization filters which allow a better separation of the real waves from randomly scattered energy [15]. The positions of the stations are listed in table 1 and plotted in figure 10.

TAB. 1: Locations and installation dates of the Apollo seismometer stations. The operation of all stations was terminated in 1977. Taken from [7].

Station	Location	Installation Date
12	3.04°S, 23.42°W	11/19/69
14	3.65°S, 17.48°W	02/05/71
15	26.08°N, 3.66°E	07/31/71
16	8.97°S, 15.51°E	04/21/72

The recorded data sets consist of the primary data which are in this case the arrival times of seismic waves and secondary data like amplitudes and polarization of incoming waves.

There are three types of natural seismic sources. Meteorite impacts which are easy to locate because they only occur on the moon's surface and are marked by their impact craters; near-surface moonquakes (or high-frequency teleseisms, HFT's) which occur between 0 km and 200 km depth; and deep focus moonquakes with depths of 800 km to 1100 km. The latter is the most common lunar seismic event. Unlike earthquakes, moonquakes are not caused by tectonic plate movement, but by tidal forces between the earth and the moon and are therefor smaller in magnitude (maximum Richter magnitudes of 5).

It is also possible to generate artificial seismic events on the moon, e.g. by deliberately crashing the S-IVB stages of several Apollo missions on the moon's surface [17] or by controlled detonations [18].

FIG. 8: Astronaut Buzz Aldrin deploys a seismometer at the *Sea of Tranquility* landing site during the Apollo 11 mission. This seismometer was operational for just three weeks. More advanced seismometers were deployed during the Apollo 12, 14, 15 and 16 missions. Taken from [16].

To gain information on the internal lunar structure which is basically the goal of lunar seismology, it is necessary to locate the source of a given seismic event in space and time which corresponds in the case of a deep focus moonquake to four degrees of freedom. That is why five or more arrival times of the same event must be observed in order to study the lunar structure. On the other hand, surface events like meteorite impacts or HFT's only require four observed arrival times since their altitude is naturally well-constrained to the surface ($z \approx 0$). For data analysis, events must be selected accordingly.

4 Data Analysis by Goins et al.

The following section will present the findings of N. R. Goins, A. M. Dainty and M. N. Toksöz in their publication *"Lunar Seismology: The Internal Structure of the Moon"* (1981) [7]. Although there are more recent articles that provide better and more sophisticated analysis methods, current results do not differ substantially from the

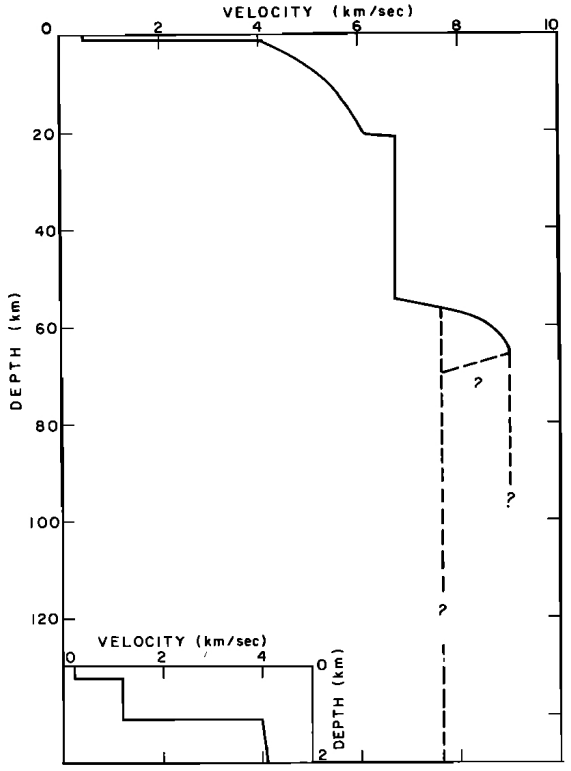

FIG. 9: Velocity model for the lunar crust used by Goins et al. in order to analyze the mantle structure. Data from [19], taken from [7].

ones shown by Goins et al. Above all, the methods presented here can be understood more intuitively and give a good idea of the problem seismologists face when analyzing seismic data.

The crustal structure of the moon has already been proposed in earlier works like the one by Cooper et al. in 1974 [19]. The results of this study are shown in figure 9 and were used by Goins et al. to account for the effect of the very low compressional wave velocities in the uppermost crust.[3]

4.1 Event Selection

As mentioned previously, seismic events must meet the requirement to allow both, localization and gain of structural information at the same time. The data set Goins et al. consequently chose, contains 8 meteoroid impacts, 8 HFT events and 24 deep moonquakes, for a total of 40 seismic events. The determined locations of these events are plotted in figure 10 together with the locations of the Apollo seismometer stations 12, 14, 15 and 16.

4.2 Analysis Methods

In principle, Goins at al. used two basic approaches to extract structural information about the moon from seismic arrival times. Both methods require that the arrival times (which are the measured quantity) are expressed as functions of the unknown parameters like event locations, origin times and, for example, vertical velocity gradients. Given that there were only four seismometer stations operational at the time of the data acquisition, there is a maximum of eight data values (known variables) for each event (for P and S arrival times).

4.2.1 Parameter Search Method

The first method used by Goins et al. was to solve the the *forward problem* many times, i.e. choosing tentative values for the unknown parameters and calculating the resulting discrepancy from the measured arrival times. This gives as many estimates for the origin time as there were data values at hand. Now, the so-called *Geiger's method* is applied, i.e. the variance e^2 of these estimated origin times (up to eight) is calculated and serves as the fit parameter to be minimized since for *one* event there should be only *one* origin time for all seismometer stations.

Afterwards, a systematical variation of the initial values (e.g. using an evolutionary algorithm) allows to scan the whole parameter space for the optimal solution in terms of the smallest value for e^2.

4.2.2 Linearized Matrix Inversion

The second method used, utilizes inverse problem theory to solve for the unknown parameters. A more detailed discussion of this method is, for instance, given by Ralph A. Wiggins [21].

[3] Actually, the velocity model by Cooper et al. applies just to the lunar crust in the Oceanus Procellarum region beneath The Apollo 12 and 14 station. However, further studies have shown that the crustal structure beneath other seismometer stations can be assumed to be similar [20].

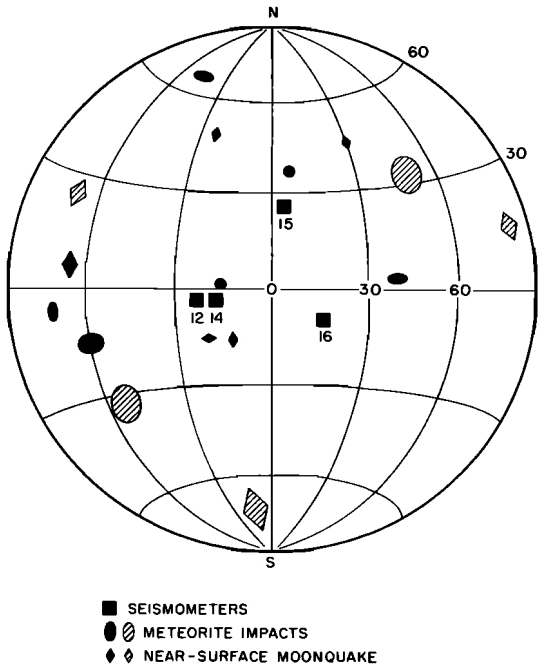

(a)

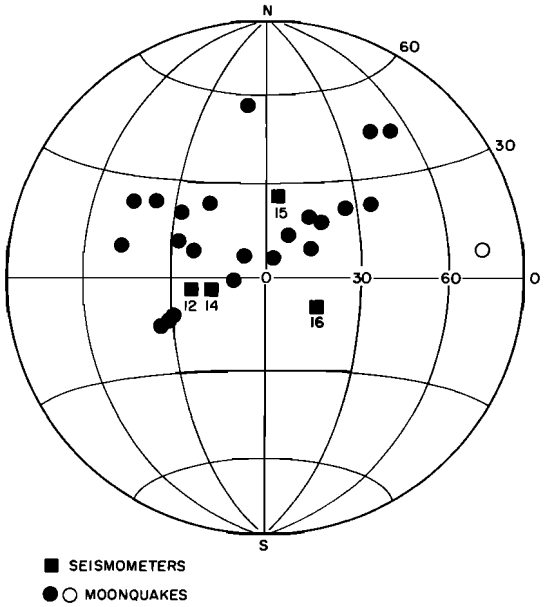

(b)

FIG. 10: The determined event locations used by Goins et al. of surface events (a) and deep moonquakes (b). Symbol size corresponds to one standard deviation in location estimate. Taken from [7].

First, a vector $\mathbf{d}$ is defined

$$\mathbf{d} = (d_1, d_2, d_3, \ldots, d_n), \tag{4.1}$$

where each component of $\mathbf{d}$ represents one measured data point (P or S arrival time). For N observed events, we get $n \leq 8N$. In the same manner, $\mathbf{b}$ represents the unknown parameters to be determined.

$$\mathbf{b} = (b_1, b_2, b_3, \ldots, b_m), \tag{4.2}$$

where m denotes the total number of unknown parameters. For I surface events, J deep moonquakes and K velocity model values, we have $m = 3I + 4J + K$ since for every surface event latitude, longitude and origin time must be determined and for interior events also depth.

For the whole data set used by Goins et al., we have $I = 16$, $J = 24$, $K = 4$, $N = 40$, $n = 228$, $m = 148$.

The initial parameter values are taken from the first parameter search approach (section 4.2.1) and denoted as $\mathbf{b}'$, whereas the resultant predicted data values are referred to as $\mathbf{d}'$ so that

$$\mathbf{d}' = F(\mathbf{b}'), \tag{4.3}$$

where F is the functional relationship between the knowns (arrival times) and the unknowns that arises from theoretical treatments like the one described in section 2. An exact description of the used ray-tracing theory can be found in [22].

Now, the misfits between the predicted and the measured arrival times are expressed as

$$\mathbf{\Delta d} = \mathbf{d} - \mathbf{d}' \tag{4.4}$$

and the corrections to the initial model values as

$$\mathbf{\Delta b} = \mathbf{b} - \mathbf{b}'. \tag{4.5}$$

Then we can describe the relation between $\mathbf{\Delta d}$ and $\mathbf{\Delta b}$ as

$$\mathbf{\Delta d} = A\mathbf{\Delta b}, \tag{4.6}$$

where A is the Jacobian matrix

$$A = \begin{pmatrix} \frac{\partial d_1}{\partial b_1} & \cdots & \frac{\partial d_1}{\partial b_m} \\ \vdots & & \vdots \\ \frac{\partial d_n}{\partial b_1} & \cdots & \frac{\partial d_n}{\partial b_m} \end{pmatrix}, \tag{4.7}$$

that can be solved for using analytical methods of linear inversion described in *"Quantitative Seismology"* by Keiiti Aki and Paul G. Richards [23].

The resulting corrections can be used to repeat at the same calculation with the refined initial values iteratively. This approach is more effective than the parameter search method which has only been used to get reasonable initial values for the first iteration.

4.3 Results

The following section will summarize the results Goins et al. came to and conclude this work. In addition to the pure velocity model that has been obtained using the methods describes above, Goins et al. were also able to figure out an attenuation model that quantifies the anelastic attenuation of a seismic wave due to friction and other energy losses depending on the depth. The quantity used in seismology to express the attenuation is the quality factor Q which is inversely proportional to the attenuation factor δ and defined as

$$Q = 2\pi \frac{E}{\Delta E}, \tag{4.8}$$

where $E/\Delta E$ denotes the energy loss per wave cycle [24]. This Q value also yields information about the lithology and other parameters such as porosity.

Experimentally, Q values can be accessed by examining the amplitudes of the measured seismic signals. Although the corresponding theoretical basics have not been discussed in this work, the results will be shown for the sake of completeness.

4.3.1 Velocity and Attenuation Model

The velocity model Goins et al. obtained in this work is tabulated in table 2 and illustrated in figure 11.

According to these data the upper mantle region ranges from 60 km to 400 km depth with average wave velocities of $v_P = (7.7 \pm 0.2)\mathrm{km\,s^{-1}}$ and $v_S = (4.45 \pm 0.05)\mathrm{km\,s^{-1}}$.

Between the upper and lower mantle regions, there is a transition zone ranging from 400 km to 480 km depth. The region below this transition zone extends to a depth of 1100 km and marks the lower mantle with average wave velocities of $v_P = (7.6 \pm 0.6)\mathrm{km\,s^{-1}}$ and $v_S = (4.2 \pm 0.1)\mathrm{km\,s^{-1}}$.

TAB. 2: Velocity model for P and S waves obtained by Goins et al. Taken from [7].

Depth [km]	v_P [$\mathrm{km\,s^{-1}}$]	v_S [$\mathrm{km\,s^{-1}}$]
60	7.75	4.57
400	7.65	4.37
480	7.6	4.20
1100	7.6	4.20

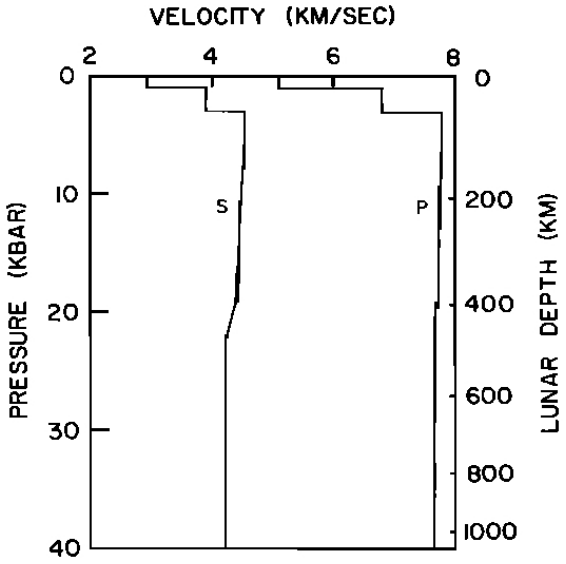

FIG. 11: Plot of the moon's velocity model (P and S waves), wave velocity in dependence of depth. Taken from [7].

Goins et al. were not able to extract any reliable information about the lunar structure below 1100 km depth (the depth of the deepest moonquakes registered) including evidence concerning the existence of a core.[4]

The attenuation model obtained from amplitude measurements is given in table 3.

Summarizing all the information stated above, we arrive at a lunar interior structure that is illustrated in figure 12.

[4] More recent works provide evidence of a lunar core, albeit of small radius (350 km or less) [25].

TAB. 3: Attenuation model obtained by Goins et al. Taken from [7].

Region	Depth [km]	Q
Crust	0–60	5000
Upper mantle	60–400	4000
Lower mantle	400–1100	1500
Attenuating zone	>1100	<500

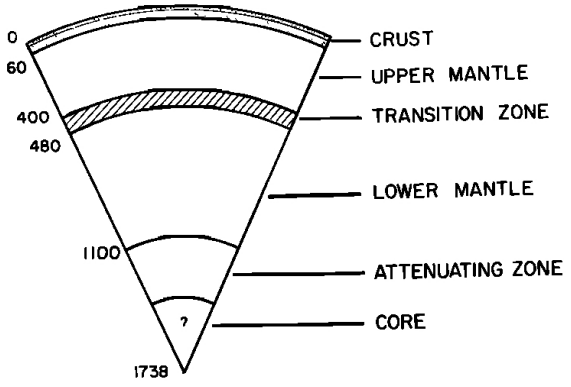

FIG. 12: Lunar interior structure after Goins et al. No reliable information about the attenuating zone and a possible core could be acquired. Taken from [7].

5 Outlook

Since the data sets provided by the Apollo Passive Seismic Experiment are limited, it will be necessary to deploy new instruments on the moon in order to gain new insights about the internal structure (all discoveries of the last years were due to more elaborate analysis methods applied to the old data sets).

One particular experiment that has often been proposed, is the installation of *seismological arrays* on the lunar surface [26]. A seismological array is basically a spacial sequence of seismometers of well-defined configuration and relative distance [27]. This array configuration has numerous advantages over single seismometers, whereat the most important one is probably the possibility to sum over all individual recordings of the array stations and therefor to obtain a significantly better signal-to-noise ratio. Furthermore, seismological arrays can gain directional information about seismic signals allowing to directly locate a seismic source with a single array

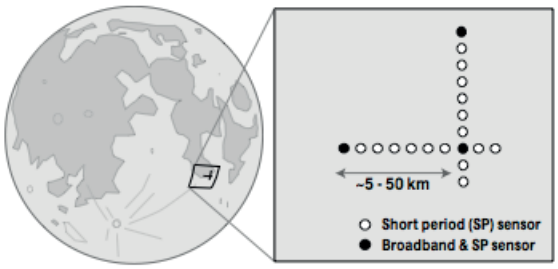

FIG. 13: Schematic of the *Small Aperture Lunar Seismic Array* (SALSA) proposed by Fouch et al. Taken from [26].

measurement [27]. A schematic of the seismological array proposed by M. J. Fouch et al. is shown in figure 13.

Thanks to the improved signal-to-noise ratio seismological arrays provide, it would be possible to lower the detection threshold and therefor record moonquakes below the current threshold of about 1100 km depth and to increase the measurement precision overall allowing to resolve the fine-structure of the moon's interior [27]. The main goal of such an experiment would probably be to determine the location and state of the moon's core which is, until now, unclear [26].

References

[1] Richard Dixon Oldham. The constitution of the interior of the earth, as revealed by earthquakes. *Quarterly Journal of the Geological Society*, 62(1–4):456–475, 1906.

[2] Andrija Mohorovičić. Potres od 8. *X*, pages 1–56, 1909.

[3] Adam M. Dziewonski and Don L. Anderson. Preliminary reference earth model. *Physics of the Earth and Planetary Interiors*, 25(4):297–356, 1981.

[4] Peter M. Shearer. *Introduction to Seismology*. Cambridge University Press, 2009.

[5] G. V. Latham, H. J. Dorman, P. Horvath, A. K. Ibrahim, J. Koyama, and Y. Nakamura. Passive seismic experiment: a summary of current status. *Lunar and Planetary IX*, pages 634–636, 1978.

[6] Yosio Nakamura, Gary V. Latham, and H. James Dorman. Apollo lunar seismic experiment–final summary. *Journal of Geophysical Research*, 87:A117–A123, 1982.

[7] N. R. Goins, A. M. Dainty, and M. N. Toksöz. Lunar seismology: The internal structure of the moon. *Journal of Geophysical Research: Solid Earth*, 86(B6):5061–5074, 1981.

[8] Feng Kang and Shi Zhong-Ci. *Mathematical Theory of Elastic Structures*. Springer Berlin Heidelberg, 1996.

[9] Rudolf Gorenflo and Sergio Vessella. Abel integral equations- analysis and applications. *Lecture Notes in Mathematics*, 1461, 1991.

[10] Harry Bateman. Die Lösung der Integralgleichung, welche die Fortpflanzungsgeschwindigkeit einer Erdbebenwelle im Inneren der Erde mit den Zeiten verbindet, die die Störung braucht, um zu verschiedenen Stationen auf der Erdoberfläche zu gelangen. *Physikal. Zeitschr.*, 11:96–99, 1910.

[11] Gustav Herglotz. Über das Benndorf'sche Problem der Fortpflanzungsgeschwindigkeit der Erdbebenstrahlen. *Physikal. Zeitschr.*, 8:145–147, 1907.

[12] Emil Wiechert and Ludwig Geiger. Bestimmung des Weges von Erdbebenwellen im Erdinneren. *Physikal. Zeitschr.*, 11:394–411, 1901.

[13] Emil Wiechert. Bestimmung des Weges von Erdbebenwellen. I. *Theoretisches Phys. Z.*, 11:294–304, 1910.

[14] Gary V. Latham, Maurice Ewing, Frank Press, George Sutton, James Dorman, Yosio Nakamura, Nafi Toksöz, Ralph Wiggins, John Derr, and Frederick Duennebier. Passive seismic experiment. *Science*, 167(3918):455–457, 1970.

[15] E. A. Flinn. Signal analysis using rectilinearity and direction of particle motion. *Proceedings of the IEEE*, 53:1874–1876, 1965.

[16] Trudy E. Bell and Tony Phillips. Moonquakes. *Science@NASA*, 2006.

[17] G. V. Latham, J. Dorman, F. Duennebier, M. Ewing, D. Lammlein, and Y. Nakamura. Moonquakes, meteoroids, and the state of the lunar interior. *Proceedings of the Lunar Science Conference*, 4:2515, 1973.

[18] M. Brzostowski and A. Brzostowski. Archiving the apollo active seismic data. *The Leading Edge*, 28(4):414–416, 2009.

[19] Michael R. Cooper, Robert L. Kovach, and Joel S. Watkins. Lunar near-surface structure. *Reviews of Geophysics*, 12(3):291–308, 1974.

[20] Neal R. Goins, Anton M. Dainty, and M. Nafi Toksöz. Structure of the lunar crust at highland site Apollo station 16. *Geophysical Research Letters*, 8(1):29–32, 1981.

[21] Ralph A. Wiggins. The general linear inverse problem: Implication of surface waves and free oscillations for earth structure. *Reviews of Geophysics*, 10(1):251–285, 1972.

[22] N. R. Goins, M. N. Toksöz, and A.M. Dainty. Seismic structure of the lunar mantle-an overview. *Lunar and Planetary Science Conference Proceedings*, 9:3575–3588, 1987.

[23] Keiiti Aki and Paul G. Richards. *Quantitative Seismology*, volume 1424. Freeman San Francisco, 1980.

[24] Robert E. Sheriff and Lloyd P. Geldart. *Exploration Seismology*, volume 2. Cambridge University Press, New York, NY, 1985.

[25] Mark A. Wieczorek, Bradley L. Jolliff, Amir Khan, Matthew E. Pritchard, Benjamin P. Weiss, James G. Williams, Lon L. Hood, Kevin Righter, Clive R. Neal, Charles K. Shearer, I. Stewart McCallum, Stephanie Tompkins, B. Ray Hawke, Chris Peterson, Jeffrey J. Gillis, and Ben Bussey. The constitution and structure of the lunar interior. *Reviews in Mineralogy and Geochemistry*, 60(1):221–364, 2006.

[26] M. J. Fouch, E. J. Garnero, M. S. Thorne, P. Lin, N. Schmerr, R. Weber, M. S. Robinson, and H. Yu. Small aperture lunar seismic arrays (SALSAs). *LPI Contributions*, 1530:3032, 2010.

[27] Sebastian Rost and Christine Thomas. Array seismology: Methods and applications. *Reviews of Geophysics*, 40(3):1008, 2002.